Robust Lignin-Based Aerogel Filters: High-Efficiency Capture of Ultrafine Airborne Particulates and the Mechanism

Zhihui Zeng,[a,#] *Xiu Yun Daphne Ma,*[a,#] *Youfang Zhang,*[a] *Zhe Wang* [a] *Bing Feng Ng,*[b] *Man Pun Wan,*[b] *and Xuehong Lu* [a,] *

[a] School of Materials Science and Engineering, Nanyang Technological University, 50 Nanyang Avenue, Singapore 639798, Singapore.

[b] School of Mechanical and Aerospace Engineering, Nanyang Technological University, 50 Nanyang Avenue, 639798, Singapore.

* E-mail: asxhlu@ntu.edu.sg (Xuehong Lu)

[#] These authors contributed equally to this work.

Keywords: Lignin, aerogel, cross-linking, wood-like microstructure, air filtration

Abstract: In this article, we report a new type of lignin-based wood-like aerogel filters composed of aligned micrometer-sized pores and cross-linked lignin-based cell walls, as well as their air filtration-related properties. The aerogel filters were prepared via facile unidirectional ice-crystal-induced self-assembly from an aqueous solution followed by annealing at 300 °C. The cross-linking of lignin and reinforcement with a very small amount of graphene significantly enhance the mechanical stiffness, thermal stability and humidity/water resistance of the aerogels. Simultaneously, abundant functional groups retained from lignin and the aligned pore channels lead to high filtration efficiency for ultrafine particles accompanied with fairly low pressure drop. Moreover, these low-cost and renewable biomass-based filters also exhibit outstanding long-term filtration efficiency. Through filtration tests with particles of various sizes, it is revealed that the air filtration by this type of aerogel filters is dominated by diffusion, rather than impaction or interception mechanism, which offers a new avenue for design of novel high-performance air filters.

Introduction

Particulate matter (PM), consisting of abundant micrometer- and nanometer-sized particles suspended in air, has caused severe air pollution, and remains an ever-growing environmental issue.[1-10] In addition to the detrimental effects of PM on our living environments in terms of visibility, radiative forcing and climate change, the particles comprising organic and inorganic compounds with trace amount of metals can give rise to adverse health effects, such as respiratory and cardiovascular diseases.[3, 9-13] Particularly, the pollutant particles with sizes of ≤ 0.1 μm (PM 0.1), commonly referred as ultrafine particles, have higher reactivity and greater potential harmful impact to the human health, and yet studies on PM 0.1 filtration materials are seldom undertaken owing to the complex issues involved.[14-19]

Much work has been conducted on conventional fibrous filters [20-22] that are composed of melt-blown fibers, glass fibers, or spun-bonded fibers because these filters are low-cost and have relatively large specific surface area for adsorption of airborne particles. Pollutant particles are deposited on the fiber surface via different filtration mechanisms including sieving, inertial impaction, interception and diffusion.[11, 23] However, higher fiber packing density is necessary for enhancing the filtration efficiency of the fibrous filters for smaller particles, especially ultrafine particles, because they are mainly captured via diffusion, i.e., the adsorption of these particles relies on their Brownian motion around the fibers[17, 18]. The high packing density inevitably leads to a surge in pressure drop (ΔP), increasing the energy consumption in filtration. A number of approaches have been used to address this issue via manipulating

microstructural characteristic of the filter and/or introducing a new constituent phase into the filtration materials.[1, 3, 6-8, 13, 24-28] For example, Liu et al. demonstrated that the filters composed of electrospun polyacrylonatrile nanofibers were able to achieve a high filtration efficiency of 98.11 % for particles with size of ≤ 2.5 μm (PM 2.5) and ΔP of 206 Pa at a high wind velocity of 0.21 m/s.[1] Li et al.[24] found that graphene oxide (GO)-induced bead-on-string morphology could promote slip flow effect, which will reduce the drag force, decreasing the overall ΔP of filters. [24, 26] It was also reported that hot-pressing metal-organic-framework powder into a crystalline coating on three-dimensional (3D) melamine foam could lead to a higher PM 2.5 filtration efficiency of 99.6% at a lower ΔP of 125 Pa as compared with commercial breathing masks with removal efficiency of 14.4 % and ΔP of >400 Pa and a wind velocity of 204 cm s^{-1}.[25] 3D highly porous nanofibrous filters could offer lower ΔP as vast amounts of pores could be formed among entangled nanofibers, allowing air molecules to flow through easily.[29-31] The 3D filters also provide increased diffusion paths within the filters, which could potentially improve the filtration efficiency for ultrafine particles that are mainly captured via diffusion [17, 18, 31]. The practical applications of such highly porous nanofibrous filters are, however, challenged by their relatively poor mechanical properties, which hampers their potentials in improving the filtration performance. Furthermore, most reported air filters are made of synthetic materials or petrochemicals.[1-3] There is, therefore, an urgent need for development of low-cost, environmentally benign air filters possessing high filtration efficiency, low ΔP and good mechanical properties.[32,33] Although biomass-derived architectures have been

explored for various applications,[34-37] they were either fabricated by carbonization at high temperatures, which were low-yield and energy-intensive processes, or prepared via chemical processes that involve organic solvents and/or harsh chemicals. High-yield production of biomass-based architectures in a more sustainable way still remains a challenge.

Inspired by natural wood, which has abundant tube channels along its growth direction, herein we propose a novel design of wood-like aerogels for air filtration applications. Wood-like materials have been prepared via various advanced nanotechnologies, including both the bottom-up self-assembly from nanocellulose or synthetic resins and the top-down approaches from wood.[38-40] Unlike the recently reported cellulose-based wood-like aerogels prepared by chemically removing lignin and hemicellulose from natural wood,[39] our wood-like aerogels are predominantly made of lignin, which is one of the most abundant biomass,[34, 36, 37] and can be obtained as a low-cost byproduct from paper industry. The lignin-based aerogels are composed of cross-linked lignin-based cell walls with micrometer-sized tube channels in between, which can efficiently reducing the air flow resistance (ΔP) of the aerogels during filtration in comparison with the air filters made of randomly entangled fibers.[8] Recent work on cross-flow filtration have showed that the aligned channels with open ends could result in a pressure drop of only about one fifth of that of conventional filtration mode.[19,28] Simulation studies also suggested that cross-flow filtration removed particle based on size-dependent trajectory segregation, where smaller particles are deposited on the filter media while the larger ones travel continuously along the air flow.[41]

However, since aligned hollow fibers typically have relatively large inner diameter (> 500 μm), the filtration efficiency calculated based on the before and after test concentrations at two ends of the hollow fibers was fairly low.[41] In this work, we hypothesized that by utilizing the aligned channels directly for air filtration (no cross-flow) and greatly reducing the tube diameters to tens of microns, the cell walls could adsorb particles in Brownian motion more efficiently, boosting the filtration efficiency for smaller particles, while the adsorption of particles on the walls of the micrometer-sized channels will not disturb air flow significantly, making the filters more clog-resistant. Furthermore, lignin has a large amount of functional groups that are of vital importance for the adsorption of airborne organic pollutants. The wood-like aerogels could be easily fabricated via unidirectional freeze-drying[42-43] and annealing-induced cross-linking. The annealing at a low temperature of 300 ℃ could result in cross-linked lignin cell walls and hence significantly enhance the stiffness and humidity/water resistance of the filters while retaining most functional groups of lignin for adsorption of pollutant particles. A small fraction of graphene (< 3 wt%) could also be introduced into the cross-linked lignin cell walls to reduce the volume shrinkage of the aerogels in the cross-linking process, maintaining the size of the aligned pores to ensure low ΔP. Herein we demonstrate that apart from improving sustainability, renewability and biodegradability, such wood-like aerogels also exhibit excellent filtration efficiency for ultrafine particles at a low ΔP, as well as good long-term filtration performance and mechanical properties, which outperform commercial fibrous filters including high-efficiency particulate arrestance (HEPA) filters. The unique filtration behavior for our

wood-like aerogels is also revealed based on the results of filtration tests using model particles of various sizes, which provides useful guidelines for further studies.

Experimental Section

Materials and Preparation of cross-linked lignin-based aerogels: Lignin aqueous solutions of various concentrations were prepared by dissolving alkali lignin (USA, TCI product number: L0082, soft lignin) in deionized water via magnetic stirring. The solutions were cast in a Teflon container with a metal base immersed in a cold source, such as liquid nitrogen or refrigerator (-20 °C), for unidirectional freezing. Unless specifically mentioned, the cold source is the liquid nitrogen with a temperature of -196 ^{o}C. In the freezing process, the temperature gradient between the top and bottom side of the solutions in the mold led to the formation of ice crystals at the bottom side and unidirectional growth of the crystals towards the top. Subsequently, the frozen samples were freeze-dried in a freeze-drying vessel (–80 ^{o}C and 10 Pa) for around 24 h, and wood-like lignin aerogels with aligned micron-sized pore channels and cell walls were obtained. The aerogels were then heated at a rate of 5 ^{o}C/min in a tube furnace and annealed at the temperature of 300 ^{o}C for 2 h under argon atmosphere, leading to the crosslink of the aerogels. The lignin-based aerogels doped with graphene were prepared using the same procedure. In order to incorporate graphene layers into the aerogel cell walls, a GO aqueous suspension (prepared by modified Hummer's method as shown in our previous work,[35] and the average lateral size of GO is around 10 μm) was mixed with lignin solutions for further freezing-drying process. The GO content in the

lignin/GO mixture was fixed at 2.7 wt%. A wide range of densities of the aerogels was achieved by simply adjusting the water fraction of the initial aqueous suspensions. Also, various shapes or sizes of the wood-like aerogels could be achieved by using various molds, satisfying a variety of application occasions. Unless mentioned, all the crosslinked samples were annealed at a temperature of 300 ℃ and the tested data were originated from these aerogels. The lignin-based aerogels were also annealed at 600 and 900 ºC for 2 h, respectively, to make a comparison with the aerogel filters annealed at 300 ºC.

Characterization: Microstructural images of the wood-like aerogels were obtained using a scanning electron microscope (SEM, JSM-7600F). The mechanical compressive curves were evaluated by a dynamic mechanical analyzer (DMA, TA Q800), and at least five samples were tested for each component. A thermogravimetric analyzer (TGA, TA Instrument Q500) was applied to realize the TGA curves. The experiment was carried out in nitrogen atmosphere. X-ray diffraction (XRD) patterns were attained by a specular reflection mode (Cu Ka radiation, PANalytical, Holland) at room temperature. The functional groups of the aerogels after drying treatment were characterized by FTIR (Spectrum One, PE, US) spectroscopy. The porosities of the aerogels were estimated from the measured density of the aerogels and the corresponding bulk materials. For details, please refer to Supporting Information.

Filtration test: For the filtration test including filtration efficiency and pressure drop of the prepared 3D aerogel filters, a testing system was designed as shown in Figure S1. In the testing process, the model haze particles were generated by burning the incense.

The PM particle concentration was controlled by diluting the incense smoke with air in a mixing chamber, down to a hazardous pollution level equivalent (400-500 μg/m^3). The particle concentration was measured simultaneously with a condensation particle counter (NanoScan SMPS 3910, TSI Instruments Ld) that could detect PM particles with size between 0.01 to 0.42 μm and an optical particle sizer (OPS 3330, TSI Instruments Ld) that could detect PM particle with size between 0.3 to 10 μm. The particle amount in airflow before and after the air inlet being covered by the filters was recorded by the particle counters, and the filtration efficiency was calculated through comparing the PM particle number before and after filters. The pressure drop was measured using a differential pressure gauge (Digital Manometer, Bluewind Laboratory Pte Ltd). The airflow to the filter was created by the use of an air pump, and the wind velocity was measured by the air velocity meter (Airflow instruments velocity meter TA430, TSI Instruments Ld). The wind velocity and humidity in the mixing chamber could both be adjusted, and unless special mentioned, the face velocity and humidity used in the filtration testing was 5.3 cm/s and 60 %, respectively. The distributions of the simulated haze model particles were presented in Figure S2. From the distribution curves, incense smoke displayed a wide distribution from 10 nm to around 500 nm, with majority of the particles with sizes less than 1 μm, and particles with sizes between 50 nm and 200nm displayed the highest number concentration. Actually, the organic/inorganic compounds found in incense smoke have shown to be more closely related to actual haze particles. [1, 44] Therefore, the adsorption of incense smoke would provide a more relevant and credible overview of the filtration efficiencies of the filters

used in this work. In this work, the filtration efficiency to ultrafine PM particles was calculated within the incense particles with size of below 0.1 μm (PM 0.1). To further study the filtration mechanism of the aerogels, aerosols of Diethylhexyl sebacate (DEHS) were generated with a Condensation Aerosol Generator (TOPAS SLG 250, Dresden, Germany). DEHS is a colourless liquid that is insoluble in water and commonly used for aerosol generation for filter testing. DEHS particles with size of 0.1, 0.2, 0.3, 0.5 and 1.0 μm were produced respectively by the generator.

Results and Discussion

The preparation process for the wood-like aerogels is illustrated in Figure 1 a-c. Briefly, unidirectional ice-crystal-induced self-assembly of lignin in an aqueous suspension leads to aligned cell walls, and a small amount of GO can be conveniently incorporated in the cell walls of the lignin-based aerogels (**Figure 1**a, b). By low-temperature (300 ℃) annealing, cross-linked cell walls, which are composed of annealed lignin (A-lignin) doped with a small fraction of GO-derived reduced graphene layers as reinforcement, can be obtained (Figure 1c). This results in excellent microstructural and macroscopic stabilities as well as outstanding mechanical strength of the A-lignin/graphene (A-lignin/G) composite aerogels, which can support a piece of metal of over two thousand times heavier without suffering significant plastic deformation (Figure 1d-e, Figure S3). Moreover, the lignin-based aerogels can be crosslinked at a low annealing temperature compared with the commonly used annealing temperature (⩾900 ℃) in traditional carbonization processes,[34,35,37,45] which is instrumental in further lowering the cost. The

assembly process leads to wood-like texture formed by micrometer-sized isotropic pores in the cross sectional plane (Figure 1f) and aligned pore channels in the longitudinal direction (Figure 1g, h). The cross-linking process of the aerogels has minimal effects on the aligned pore channels, but leads to rougher surface and smaller thickness of cell walls (Figure 1g-j). Compressive stress-strain curves of the aerogels show the significant roles of initial concentration, cross-linking and the presence of graphene layers play in enhancing the mechanical strength of the aerogels (Figure 1k). Obviously, higher lignin concentrations contribute more building blocks to the resultant aerogels and hence give higher modulus. The low-temperature annealing-induced cross-linking and incorporation of a low fraction of graphene layers can also lead to significant mechanical enhancement of the aerogels, respectively. Furthermore, the thermal stability of the aerogels is also significantly enhanced via annealing, and it increases with the annealing temperature, as shown in Figure 1l.

The thermogravimetric analysis (TGA)/differential thermal gravity (DTG) curves, X-ray diffraction (XRD) patterns, and Fourier transform infrared (FTIR) spectra of the wood-like aerogels provide further evidence for the occurrence of cross-linking and its influence. Lignin consists of macromolecules with three-dimensional links among their methoxylated aromatic units. The TGA/DTG curves of lignin-based aerogels show three typical regions (Figure 1l).[35, 45] The first weight loss stage in the temperature range from 40 to 100 °C corresponds to the evaporation of the water absorbed, which also implies the presence of plentiful hydrophilic functional groups in the aerogels. The weight loss at around 300 °C can be mainly attributed to the cleaving of alkyl and

methoxy groups in the pyrolysis process, releasing methanol and phenolic compounds with hydroxyl group and alkyl groups. At the temperatures above 600 °C, the decarbonylation reaction of alkyl side chains and significant reduction of functional groups could occur, facilitating the formation of amorphous carbon. Therefore, XRD patterns of the A-lignin-based aerogels annealed at 300 and 600 °C show a sharp peak at $2\theta = 22.5°$, which is similar to that of the lignin-based aerogels, while those annealed at 900 °C show a broad peak at $2\theta = \sim 24.5°$ that corresponds to amorphous carbon (**Figure 2**a). FTIR studies (Figure 2b, Figure S4) further confirm the structural change of the lignin/GO composites caused by annealing. After annealing at 300 ^{o}C, the intensity of the C-H stretching band at around 2937 cm^{-1}, which corresponds to aromatic methoxyl groups as well as in methyl and methylene groups of side chains, is decreased significantly. This can be attributed to the reduction reactions of these groups. The bands at 1043-1073 cm^{-1}, which can be ascribed to C-O stretching, also weaken, indicating the breakage of some C-O bonds. By contrast, the annealing at 600 °C results in the loss of many functional groups, causing a large intensity reduction of many bands. The band at 1639 cm^{-1} (C=C) indicates that there is still a significant amount of the aromatic rings retained in the structure. However, the band at around 1736 cm^{-1}, which is ascribed to C=O bonds, are not observed, implying that most of the C=O are cleaved. The FTIR spectrum of the aerogels after annealing at 900 °C shows a relatively flat curve with no obvious band, indicating that most of the functional groups have been converted to amorphous carbon. In short, the functional groups that can interact with PM particles are reduced with increased annealing temperature, and almost removed

for the A-lignin-based aerogels annealed at 900 °C. In addition, higher annealing temperatures also lead to much low product yields, and larger volume shrinkage of the aerogels because of the massive weight reduction of the lignin in the annealing process. The shrinkage can lead to the reduction of the filtration efficiency for ultrafine PM particles yet increase the ΔP (Figure 2c, Figure S1, Figure S2). Without annealing, the lignin-based aerogels show a higher ΔP and relatively lower filtration efficiency than the A-lignin-based aerogels annealed at 300 °C because the former have a lower porosity (Table S1) and smoother cell walls that are not beneficial for adsorption of PM particles. Furthermore, the uncross-linked lignin-based aerogels are too fragile to be used for filtration, which often results in sample breaking down in the testing process. More importantly, the A-lignin-based aerogels can well retain its integrity after being immersed in water for more than 20 hours, while the lignin-based aerogels are dissolved immediately upon contacting with water (Figure 2d, Figure S5). Therefore, the A-lignin-based aerogels are able to exhibit a stable ΔP in an extremely high-humidity environment of 95 % RH for over 20 hours. The excellent water/humidity resistance of the A-lignin-based aerogels render the aerogels suitable for high-humidity filtration environments.

Many factors such as the wood species or climate can have influence on the pore size and the wall thickness of natural woods.[38] Similarly, the porosity, pore size, and cell wall thickness of the lignin-based aerogels created using the ice-templated freeze-drying method can also be adjusted by changing parameters such as lignin concentration, graphene reinforcement and freezing temperature. Higher lignin

concentration in the suspension can increase the amount of building blocks in the aerogels, contributing to higher density and lower porosity. Interestingly, the presence of a small amount of graphene leads to a lower density (higher porosity) for the A-lignin-based aerogels, which can be attributed to the mechanical enhancement of cell walls that result in a smaller volume shrinkage of the macroscopic aerogels **(**Figure 3a). Higher initial lignin concentration, which causes lower porosity of the aerogels, leads to higher filtration efficiency due to the presence of more functional groups in the A-lignin-based aerogels. Differently, the presence of graphene affects the filtration efficiency slightly but significantly reduces the ΔP (Figure 3b). For example, the ΔP values are 16.5 Pa and 32.9 Pa, respectively, for the A-lignin/G and A-lignin aerogels prepared from 5 wt% lignin-based suspension, while both show similar filtration efficiencies values of above 90 %. In addition to the smaller macroscopic shrinkage, the A-lignin/G aerogels with mechanically enhanced cell walls also show more aligned and regular pore channels than those of the A-lignin aerogels (Figure 3c-d, Figure S6), which is beneficial for the flow of air molecules and the reduction of ΔP. Therefore, the ΔP can be lowered down to 5.5 Pa by adjusting the initial lignin concentration of the A-lignin-based aerogels, which is accompanied by at a relatively high filtration efficiency of over 70 % for ultrafine particles. Moreover, it should also be mentioned that it may be possible to replace the GO with other types of reinforcements, such as exfoliated clay or recycled cellulose fibers, to improve the mechanical properties of the cell walls in the lignin aerogels, further lowering the cost of the air filters as well as making them more sustainable and biodegradable.

The filtration efficiency can also be increased significantly by increasing the thickness of the filters, which gives a slight increase of the ΔP due to the aligned pore channels (Figure 3e). The filtration efficiency reaches 96.5 %, an efficiency level comparable to that of the reference HEPA filter (over 95 %), while the ΔP is only 24 Pa for the wood-like aerogels at a thickness of 4.2 mm. When the thickness of the A-lignin/G aerogels prepared from 5.0 wt% lignin suspension is increased to 8 mm, the efficiency reaches a value of 99.85 % at a low ΔP of 45 Pa. By controlling the lignin concentration or thickness of the aerogels, the efficiency and ΔP can be fine-tuned to satisfy various filtration applications. For example, the efficiency of the A-lignin/G aerogels prepared from 3.6 wt% lignin suspension can be adjusted to 99.97 % at a thickness of 12 mm and ΔP of 74 Pa.

The freezing temperature can also be controlled to adjust the microstructure of the aerogels, which gives rise to different filtration performance (Figure 3f). Higher freezing temperature such as -20 ℃ leads to less ice-crystal nuclei at the bottom of the suspension and hence thicker ice crystals. [42, 46] The average pore size is obviously larger and the cell walls are thicker (Figure 3g, h, Figure S7). Therefore, the aerogels frozen at a higher temperature exhibit lower ΔP and filtration efficiency owing to the reduced overall amount of functional groups on the surface of thicker cell walls. It is also observed that aerogels prepared at a lower lignin concentration and different freezing temperatures show smaller difference in their ΔP values, which can be ascribed to their extremely high porosity. Moreover, it should be mentioned that the filtration efficiency of the aligned porous aerogel filters prepared by freezing at -20 ^{o}C is still reasonably

high with a fairly low pressure drop. This implies that a much higher freezing temperature than -196 ^{o}C may also give desired microstructures. In short, the high filtration efficiency for ultrafine particles and low ΔP of the wood-like aerogels, as well as their tailorability through facile adjustment of porosity, pore size, cell wall thickness and filter thickness, make the aerogels very attractive for filtration applications.

Testing condition such as the wind velocity in the testing system can also affect the filtration performance, as shown in Figure 4a. Higher testing wind velocity results in higher air flow resistance and lower filtration efficiency. The filtration efficiency can be reduced from 99.85 to 99.62 % with a wind velocity increased from 5.3 to 14.1 cm/s due to the decreased residence time of air pollutants in the filters, and the ΔP is increased from 45 to 132 Pa. Figure 4b shows the comparison of the filtration performance in terms of filtration efficiency, ΔP, and calculated quality factor (QF) of the wood-like aerogels with those of commercial filters, including high-efficiency air filters (H13 and H11), medium-efficiency filters (F7), and low-efficiency filters (G4), tested under the same condition (wind velocity is 10.0 cm/s). The quality factor (QF) is used to assess the overall filtration performance of the air filters, which can be calculated using equestion $QF=-(\ln(1-\eta))/\Delta P$, where η is the filtration efficiency.[1,2,19,28] The specifications of these reference filters are given in Figure S8 and Table S2. Compared with G4, F7 and H11 filters, our aerogels can be tuned to achieve a higher filtration efficiency with a similar ΔP or a comparable filtration efficiency with a smaller ΔP, and hence a higher QF value. In comparison with H13 filters with a relatively high filtration efficiency (99.67 %) and ΔP (91 Pa), our aerogels

exhibit filtration efficiency of 99.75 % at a ΔP of 90 Pa, thus a higher QF value is achieved. In addition, despite the much larger thickness (8-12 mm) of the wood-like aerogels, their ΔP is significantly lower than or comparable to those of commercial filters or most air filters reported in literature. As discussed earlier, the aerogels with large thickness of 8 to 12 mm could exhibit ΔP of lower than 40 Pa at a wind velocity of 5.3 cm/s, which is in contrast to some reported fibrous filters such as thin polyacrylonitrile/silica nanofibrous membranes that has ΔP of 117 Pa at the wind velocity of 5.1 cm/s, [47] bead-on-string poly(lactic acid) fibrous membranes with ΔP of 165 Pa at the wind velocity of 5.8 cm/s,[48] and a 20-μm-thick polyamide nanofiber membrane with ΔP of 111 Pa at the wind velocity of 1.92 cm/s.[49] The excellent air permeability of our wood-like aerogels can be ascribed to their highly porous structure and aligned pore channels.

Figure 5a shows the filtration efficiencies of the wood-like aerogel and H13 HEPA filters as a function of filtration time (up to 600 min). The unique morphological and surface chemistry characteristics of the lignin-based aerogels give rise to excellent filtration efficiency over a long period of time as the adsorption on lignin-based cell walls is mainly dependent on the affinity of the cell walls to the test particles that are composed of polar organic compounds. By contrast, although HEPA filters exhibit high filtration efficiency initially, the efficiency decays fairly fast, which is similar to that reported by Souzandeh *et al*.[50] The likely reason is that the deposited particles diminish the electrostatic effects of the HEPA filters that are made of glass fibers. Figures 5b and 5c show the morphology of the aerogels after the adsorption of the pollutant gas

generated by burning incense. Apart from the well retained pore channels and cell walls, abundant adsorbed particles with similar size to that of the test particles (Figure S2) are observed, showing the capability of the wood-like aerogels for efficient adsorption of fine and ultrafine particles. From Figure 5b, we can also deduce that the adsorption on cell walls would not easily cause pore-clogging. By contrast, the high fiber packing density of HEPA filters may easily cause clogging of small pores.[31, 50] In short, the long-term filtration performance and clogging-resistant potential of our wood-like aerogels make them appealing to high-capacity air filtration applications.

In order to better understand the filtration mechanism of this new class of aerogels, model particles with dominant size of 0.1, 0.2, 0.3, 0.5 and 1.0 μm are used in the filtration tests (Figure 6a). Obviously, the filtration efficiency behavior of the wood-like aerogels is distinctly different from that of H13 HEPA filters (Figure 6b), which are made of randomly entangled microfibers[5, 31, 50]. For the HEPA filters, the dominant filtration mechanism for ultrafine particles with size of $\leq$ 0.1 μm is diffusion. The ultralfine particles show significant Brownian diffusion (random motion caused by the collision with gas molecules), leading to its relatively high capture efficiency. However, the particles with size of $\geq$ 0.5 μm can also be captured easily because of interception and inertial impaction (the particles directly hit the fibers instead of changing moving direction with the air flow). Thus the particles with size of around 0.3 μm are the most penetrating ones for the conventional fibrous HEPA filters. [26, 51, 52] This is in general consistent with our tested results that the particles with size of larger than 0.3 μm show significantly higher filtration efficiency than the 0.1-0.3 μm particles for HEPA filters.

The roughly comparable efficiency for 0.1-0.3 μm particles is probably due to the use of organic model particles (less charged) in the tests. Unlike conventional fibrous filters that have random pores (Figure S8), our lignin-based aerogels have aligned pore channels with the lateral size of 20-40 μm. Thus, the filtration by the lignin-based aerogel filters is more dependent on diffusion mechanism, while the inertial impaction and interception play less important roles owing to the aligned pore channels. 0.1 μm particles tend to make random motion due to their collision with gas molecules, leading to a zig-zag motion path in the filter (Figure 6c). As a result, the probability of these particles interacting with the cell walls is high and therefore, the filtration efficiency for 0.1 μm particles is the highest. As the particle size increases, the particle mass and inertia increase, and hence the particles exhibit straighter and straighter motion path. Owing to the diminished diffusion mechanism, the probability of adsorption of relatively large particles on the walls of the aligned pores is lower, causing the decrease of filtration efficiency with increasing particle size in the range of 0.1-1.0 μm. Furthermore, it is observed that for the wood-like aerogels with a relatively large thickness the filtration efficiency decreases only slightly with increasing particle size (in the range of 0.1-1.0 μm). For example, the filtration efficiency only reduce from 99.75 % for 0.1 μm particles to 99.16 % for 0.5 μm particles and 99.10 % for 1.0 μm particles. This may be attributed to the longer pore channels that could increase particle residence time and hence capture more particles with a relatively small degree of Brownian motion. Therefore, it can be concluded that excellent filtration efficiency for PM particles with a wide range of particle size can be achieved by adjusting the

processing parameters in the preparation process. It is worth noting that the trend we observed for air filters with aligned channels, i.e., efficiency decreases with particle size, is supported by experimental and simulation work reported by Sibanda et al. for cross-flow filtration, which showed that that finer particles have higher tendency to be deposited on the filter wall when the pore channels were "more opened" under low cross-flow ratios. [41]Thus, our results also demonstrate that microstructures of the filters can affect the filtration mechanism. The air filters with aligned channels can more effectively capture smaller particles in Brownian motion at a low pressure drop, improving quality factor of the filters. This work hence provides a new avenue for the design of high-performance air filters for applications where the targeted pollutant particles are smaller than 1 μm. They may also be combined with HEPA filters for improving filtration efficiency for ultrafine particles.

Conclusions

A type of wood-like aerogels with composite cell walls composed of cross-linked lignin and a small fraction of graphene, and aligned micrometer-sized pores are readily fabricated via facile unidirectional ice-crystal-induced self-assembly followed by low-temperature annealing. The specially designed aligned pore channels improve the ease of air flow, efficiently reducing the ΔP of the aerogels in filtration. The low-cost, readily available and renewable biomass, lignin, could be effectively cross-linked via annealing at 300 °C, which significantly enhances mechanical strength, thermal stability and water/humidity resistance of the aerogels, while retaining abundant functional groups

for adsorption of pollutant particles. Furthermore, the small amount of graphene layers doped in the cross-linked lignin enhance stiffness of the aerogels, reduce the volume shrinkage of the aerogels during the cross-linking process and improve the microstructures, ultimately reducing the pressure drop of the wood-like aerogels and making the aerogels mechanically robust. In short, the microstructures of the aerogel filters, including their porosity, pore size, cell wall constituent and thickness, as well as their macroscopic shapes, can be easily adjusted to tune the filtration efficiency and pressure drop. The filtration test results show that the aerogel filters exhibit a combination of outstanding long-term filtration efficiency for ultrafine particles and low pressure drop, which are better than that of commercial HEPA filters. Furthermore, through the filtration tests with particles of various sizes, a unique air filtration behavior is demonstrated for the aerogels, offering a new avenue for design of sustainable high-performance filters.

ASSOCIATED CONTENT

(S) Supporting Information

Schematic diagram and optical images of filtration testing system, number concentration-size distribution curves of the incense particles, optical and SEM images and FTIR curves of the lignin-based aerogels, and SEM images and Talbe including the information of the commercial filter materials are included in the **Supporting**

Information, which is available free of charge on the **ACS Publications website** at **http://pubs.acs.org**.

AUTHOR INFORMATION

Corresponding Author

E-mail: asxhlu@ntu.edu.sg (Xuehong Lu).

Conflicts of interest

There are no conflicts of interest to declare

ACKNOWLEDGMENTS

Z. Zeng and X.Y.D. Ma contributed equally to this work. This work was supported by Science and Engineering Research Council of the Agency for Science, Technology and Research (A*STAR) Singapore under Public Sector Research Funding (PSF) Grant No. 1521200077 and by the Republic of Singapore's Ministry of Education MOE2016-T2-1-063.

REFERENCES

(1) Liu, C.; Hsu, P. C.; Lee, H. W.; Ye, M.; Zheng, G.; Liu, N.; Li, W.; Cui, Y. Transparent air filter for high-efficiency PM2.5 capture. *Nat. Commun.* **2015,** *6*, 6205.

(2) Xu, J.; Liu, C.; Hsu, P. C.; Liu, K.; Zhang, R.; Liu, Y.; Cui, Y. Roll-to-Roll Transfer of Electrospun Nanofiber Film for High-Efficiency Transparent Air Filter. *Nano Lett.* **2016,** *16,* 1270-1275..

(3) Zhang, R.; Liu, C.; Hsu, P. C.; Zhang, C.; Liu, N.; Zhang, J.; Lee, H. R.; Lu, Y.; Qiu, Y.; Chu, S.; Cui, Y. Nanofiber Air Filters with High-Temperature Stability for Efficient PM2.5 Removal from the Pollution Sources. *Nano Lett.* **2016,** *16,* 3642-3649..

(4) Zhang, Q.; Jiang, X.; Tong, D.; Davis, S. J.; Zhao, H.; Geng, G.; Feng, T.; Zheng, B.; Lu, Z.; Streets, D. G.; et al. Transboundary health impacts of transported global air pollution and international trade. *Nature* 2017, **543**, 705-709.

(5) Xiong, Z.-C.; Yang, R.-L.; Zhu, Y.-J.; Chen, F.-F.; Dong, L.-Y. Flexible hydroxyapatite ultralong nanowire-based paper for highly efficient and multifunctional air filtration. *J. Mater. Chem. A* **2017,** *5,* 17482-17491.

(6) Zhang, S.; Liu, H.; Zuo, F.; Yin, X.; Yu, J.; Ding, B. A Controlled Design of Ripple-Like Polyamide-6 Nanofiber/Nets Membrane for High-Efficiency Air Filter. *Small* 2017, **13**, 1603151.

(7) Wang, S.; Zhao, X.; Yin, X.; Yu, J.; Ding, B. Electret Polyvinylidene Fluoride Nanofibers Hybridized by Polytetrafluoroethylene Nanoparticles for High-Efficiency Air Filtration. *ACS Appl. Mater. Inter.* **2016,** *8,* 23985-23994.

(8) Zhang, S.; Sun, J.; Hu, D.; Xiao, C.; Zhuo, Q.; Wang, J.; Qin, C.; Dai, L. Large-sized graphene oxide/modified tourmaline nanoparticle aerogel with stable honeycomb-like structure for high-efficiency PM2.5 capture. *J. Mater. Chem. A* **2018,** *6,* 16139-16148.

(9) Zhang, Y.; Yuan, S.; Feng, X.; Li, H.; Zhou, J.; Wang, B. Preparation of Nanofibrous Metal-Organic Framework Filters for Efficient Air Pollution Control. *J. Amer. Chem. Soc.* **2016,** *138,* 5785-5788.

(10) Bai, Y.; Han, C. B.; He, C.; Gu, G. Q.; Nie, J. H.; Shao, J. J.; Xiao, T. X.; Deng, C. R.; Wang, Z. L. Washable Multilayer Triboelectric Air Filter for Efficient Particulate Matter PM2.5 Removal. *Adv. Funct. Mater.* 2018, **28**, 1706680.

(11) Choi, D. Y.; Jung, S. H.; Song, D. K.; An, E. J.; Park, D.; Kim, T. O.; Jung, J. H.; Lee, H. M. Al-Coated Conductive Fibrous Filter with Low Pressure Drop for Efficient Electrostatic Capture of Ultrafine Particulate Pollutants. *ACS Appl. Mater. Inter.* **2017,** *9,* 16495-16450.

(12) Rao, C.; Gu, F.; Zhao, P.; Sharmin, N.; Gu, H.; Fu, J. Capturing PM2.5 Emissions from 3D Printing via Nanofiber-based Air Filter. *Sci. Rep.* 2017, **7,** 10366.

(13) Bian, Y.; Wang, R.; Wang, S.; Yao, C.; Ren, W.; Chen, C.; Zhang, L. Metal–organic framework-based nanofiber filters for effective indoor air quality control. *J. Mater. Chem. A* **2018,** *6,* 15807-15814.

(14) Timonen, K. L.; Vanninen, E.; de Hartog, J.; Ibald-Mulli, A.; Brunekreef, B.; Gold, D. R.; Heinrich, J.; Hoek, G.; Lanki, T.; Peters, A.; et al. Effects of ultrafine and fine particulate and gaseous air pollution on cardiac autonomic control in subjects with coronary artery disease: The ULTRA study. *J. Exp. Sci. Environ. Epid.* 2005, **16,** 332-341.

(15) Tobias, A.; Rivas, I.; Reche, C.; Alastuey, A.; Rodriguez, S.; Fernandez-Camacho, R.; Sanchez de la Campa, A. M.; de la Rosa, J.; Sunyer, J.; Querol, X. Short-term effects

of ultrafine particles on daily mortality by primary vehicle exhaust versus secondary origin in three Spanish cities. *Environ. Intern.* **2018,** *111,* 144-151.

(16) Ostro, B.; Hu, J.; Goldberg, D.; Reynolds, P.; Hertz, A.; Bernstein, L.; Kleeman, M. J. Associations of mortality with long-term exposures to fine and ultrafine particles, species and sources: results from the California Teachers Study Cohort. *Environ. Health Perspect.* **2015,** *123,* 549-546.

(17) Zhang, S.; Liu, H.; Yu, J.; Luo, W.; Ding, B. Microwave structured polyamide-6 nanofiber/net membrane with embedded poly(m-phenylene isophthalamide) staple fibers for effective ultrafine particle filtration. *J. Mater. Chem. A* **2016,** *4,* 6149-6157.

(18) Li, M.; Feng, Y.; Wang, K.; Yong, W. F.; Yu, L.; Chung, T. S. Novel Hollow Fiber Air Filters for the Removal of Ultrafine Particles in PM2.5 with Repetitive Usage Capability. *Environ. Sci. Technol.* **2017,** *51,* 10041-10049.

(19) Wang, L.-Y.; Yu, L.E.; Lai, J.Y.; Chung, T.S. Developing ultra-high gas permeance PVDF hollow fibers for air filtration applications. *Sep. Pur. Technol.* **2018**, *205,* 184-195.

(20) Chen, C. Y. Filtration of Aerosols By Fibrous Media. *Chem. Rev.* **1955,** *55,* 595-623.

(21) Uppal, R.; Bhat, G.; Eash, C.; Akato, K. Meltblown nanofiber media for enhanced quality factor. *Fiber Polym.* **2013,** *14,* 660-668.

(22) Thomas, D.; Penicot, P.; Contal, P.; Leclerc, D.; Vendel, J. Clogging of fibrous filters by solid aerosol particles Experimental and modelling study. Chem. *Eng. Sci.* **2001,** *56,* 3549-3561.

(23) Zhang, S.; Shim, W. S.; Kim, J. Design of ultra-fine nonwovens via electrospinning of Nylon 6: Spinning parameters and filtration efficiency. *Mater. Design* **2009,** *30,* 3659-3666..

(24) Li, J.; Zhang, D.; Yang, T.; Yang, S.; Yang, X.; Zhu, H. Nanofibrous membrane of graphene oxide-in-polyacrylonitrile composite with low filtration resistance for the effective capture of PM 2.5. *J. Membr. Sci.* **2018,** *551,* 85-92.

(25) Wang, A.; Fan, R.; Zhou, X.; Hao, S.; Zheng, X.; Yang, Y. Hot-Pressing Method To Prepare Imidazole-Based Zn(II) Metal-Organic Complexes Coatings for Highly Efficient Air Filtration. *ACS Appl. Mater. Inter.* **2018,** *10,* 9744-9755.

(26) Li, P.; Wang, C.; Zhang, Y.; Wei, F. Air filtration in the free molecular flow regime: a review of high-efficiency particulate air filters based on carbon nanotubes. *Small* **2014,** *10,* 4543-4561.

(27) Jiang, S.; Hou, H.; Agarwal, S.; Greiner, A. Polyimide Nanofibers by "Green" Electrospinning via Aqueous Solution for Filtration Application. *ACS Sustainable Chem. Eng.* **2016**, *4*, 4797−4804

(28) Wang, L.Y.; Yong, W.F.; Yu, L.E.; Chung, T.S. Design of high efficiency PVDF-PEG hollow fibers for air filtration of ultrafine particles. *J. Membr. Sci.* **2017**, *535*, 342-349.

(29) Zhang, Y. G.; Zhu, Y. J.; Xiong, Z. C.; Wu, J.; Chen, F. Bioinspired Ultralight Inorganic Aerogel for Highly Efficient Air Filtration and Oil-Water Separation. *ACS Appl. Mater. Inter.* **2018,** *10*, 13019-13027.

(30) Qian, Z.; Wang, Z.; Chen, Y.; Tong, S.; Ge, M.; Zhao, N.; Xu. Superelastic and ultralight polyimide aerogels as thermal insulators and particulate air filters. *J. Mater. Chem. A* **2018,** *6,* 828-832.

(31) Deuber, F.; Mousavi, S.; Federer, L.; Hofer, M.; Adlhart, C. Exploration of Ultralight Nanofiber Aerogels as Particle Filters: Capacity and Efficiency. *ACS Appl. Mater. Inter.* **2018,** *10,* 9069-9076.

(32) Fan, X.; Wang, Y.; Kong, L.; Fu, X.; Zheng, M.; Liu, T.; Zhong, W.H., Pan, S. A Nanoprotein-Functionalized Hierarchical Composite Air Filter. *ACS Sustainable Chem. Eng.* **2018**, *6*, 11606−11613

(33) Souzandeh, H.; Scudiero, L.; Wang, Y.; Zhong, W. H. A Disposable Multi-Functional Air Filter: Paper Towel/Protein Nanofibers with Gradient Porous Structures for Capturing Pollutants of Broad Species and Sizes. *ACS Sustainable Chem. Eng.* **2017**, *5*, 6209−6217

(34) Si, Y.; Wang, X.; Yan, C.; Yang, L.; Yu, J.; Ding, B. Ultralight Biomass-Derived Carbonaceous Nanofibrous Aerogels with Superelasticity and High Pressure-Sensitivity. *Adv. Mater.* **2016,** *28,* 9512-9518.

(35) Li, H.; Yuan, D.; Tang, C.; Wang, S.; Sun, J.; Li, Z.; Tang, T.; Wang, F.; Gong, H.; He, C. Lignin-derived interconnected hierarchical porous carbon monolith with large areal/volumetric capacitances for supercapacitor. *Carbon* **2016,** *100,* 151-157.

(36) Wang, S. X.; Yang, L.; Stubbs, L. P.; Li, X.; He, C. Lignin-derived fused electrospun carbon fibrous mats as high performance anode materials for lithium ion batteries. *ACS Appl. Mater. Inter.* **2013,** *5,* 12275-12282.

(37) Zeng, Z.; Zhang, Y.; Ma, X.Y.M.; Seyed Shahabadi, S.I.; Che, B.; Wang, P; Lu, X. Biomass-based honeycomb-like architectures for preparation of robust carbon foams with high electromagnetic interference shielding performance. *Carbon*, 201*8*, **140**, 227-236.

(38) Jiang, F.; Li, T.; Li, Y.; Zhang, Y.; Gong, A.; Dai, J.; Hitz, E.; Luo, W.; Hu, L. Wood-Based Nanotechnologies toward Sustainability. *Adv. Mater.* 2018, **30**, 1703453.

(39) Song, J.; Chen, C.; Yang, Z.; Kuang, Y.; Li, T.; Li, Y.; Huang, H.; Kierzewski, I.; Liu, B.; He, S.; et al. Highly Compressible, Anisotropic Aerogel with Aligned Cellulose Nanofibers. *ACS Nano* ***2018***, *12*, 1, *140*-147.

(40) Yu, Z.-L.; Yang, N.; Zhou, L.-C.; Ma, Z.-Y.; Zhu, Y.-B.; Lu, Y.-Y.; Qin, B.; Xing, W.-Y.; Ma, T.; Li, S.-C.; et al. Bioinspired polymeric woods. *Sci. Adv.* **2018**, *4*, eaat7223.

(41) Sibanda, V.; Greenwood, R.W.; Seville, J. P. K.; Ding, Y.; Iyuke, S. Predicting particle segregation in cross-flow gas filtration. *Powder Technol.* **2010**, *203*, 419-427.

(42) Zeng, Z.; Jin, H.; Chen, M.; Li, W.; Zhou, L.; Zhang, Z. Lightweight and Anisotropic Porous MWCNT/WPU Composites for Ultrahigh Performance Electromagnetic Interference Shielding. *Adv. Funct. Mater.* **2016,** *26,* 303-310.

(43) Deville, S.; Saiz, E.; Nalla, R. K.; Tomsia, A. P. Freezing as a Path to Build Complex Composites. *Science* **2006,** *311*, 515-518.

(44) See, S. W.; Balasubramanian, R.; Rianawati, E.; Karthikeyan, S.; Streets, D. G. Characterization and Source Apportionment of Particulate Matter ≤ 2.5 μm in Sumatra,

Indonesia, during a Recent Peat Fire Episode. *Environ. Sci. Technol.* **2007,** *41,* 3488-3494.

(45) Cao, J.; Xiao, G.; Xu, X.; Shen, D.; Jin, B. Study on carbonization of lignin by TG-FTIR and high-temperature carbonization reactor. *Fuel Proc. Technol.* **2013,** *106,* 41-47.

(46) Zeng, Z.; Jin, H.; Chen, M.; Li, W.; Zhou, L.; Xue, X.; Zhang, Z. Microstructure Design of Lightweight, Flexible, and High Electromagnetic Shielding Porous Multiwalled Carbon Nanotube/Polymer Composites. *Small* 2017, **13**, 1701388.

(47) Wang, N.; Si, Y.; Wang, N.; Sun, G.; El-Newehy, M.; Al-Deyab, S. S.; Ding, B. *Sep. Pur. Technol.* Multilevel structured polyacrylonitrile/silica nanofibrous membranes for high-performance air filtration. **2014,** *126,* 44-51.

(48) Wang, Z.; Zhao, C.; Pan, Z. Porous bead-on-string poly(lactic acid) fibrous membranes for air filtration. *J. Coll. Inter. Sci.* **2015,** *441,* 121-129.

(49) Liu, B.; Zhang, S.; Wang, X.; Yu, J.; Ding, B. Efficient and reusable polyamide-56 nanofiber/nets membrane with bimodal structures for air filtration. *J. Coll. Inter. Sci.* **2015,** *457,* 203-211.

(50) Souzandeh, H.; Johnson, K. S.; Wang, Y.; Bhamidipaty, K.; Zhong, W. H. Soy-Protein-Based Nanofabrics for Highly Efficient and Multifunctional Air Filtration. *ACS Appl. Mater. Inter.* **2016,** *8,* 20023-20031.

(51) Bharhate, R. S.; Ramakrishna, S. Nanofibrous filtering media: filtration problems and solutions from tiny materials. *J. Membr. Sci.* **2007**, *269,* 1-8.

(52) Podgórski, A.; Bałazy, A.; Gradón, L. Application of nanofibers to improve the filtration efficiency of the most penetrating aerosol particles in fibrous filters. *Chem. Eng. Sci.* **2006**, *61*, 6804-6815.

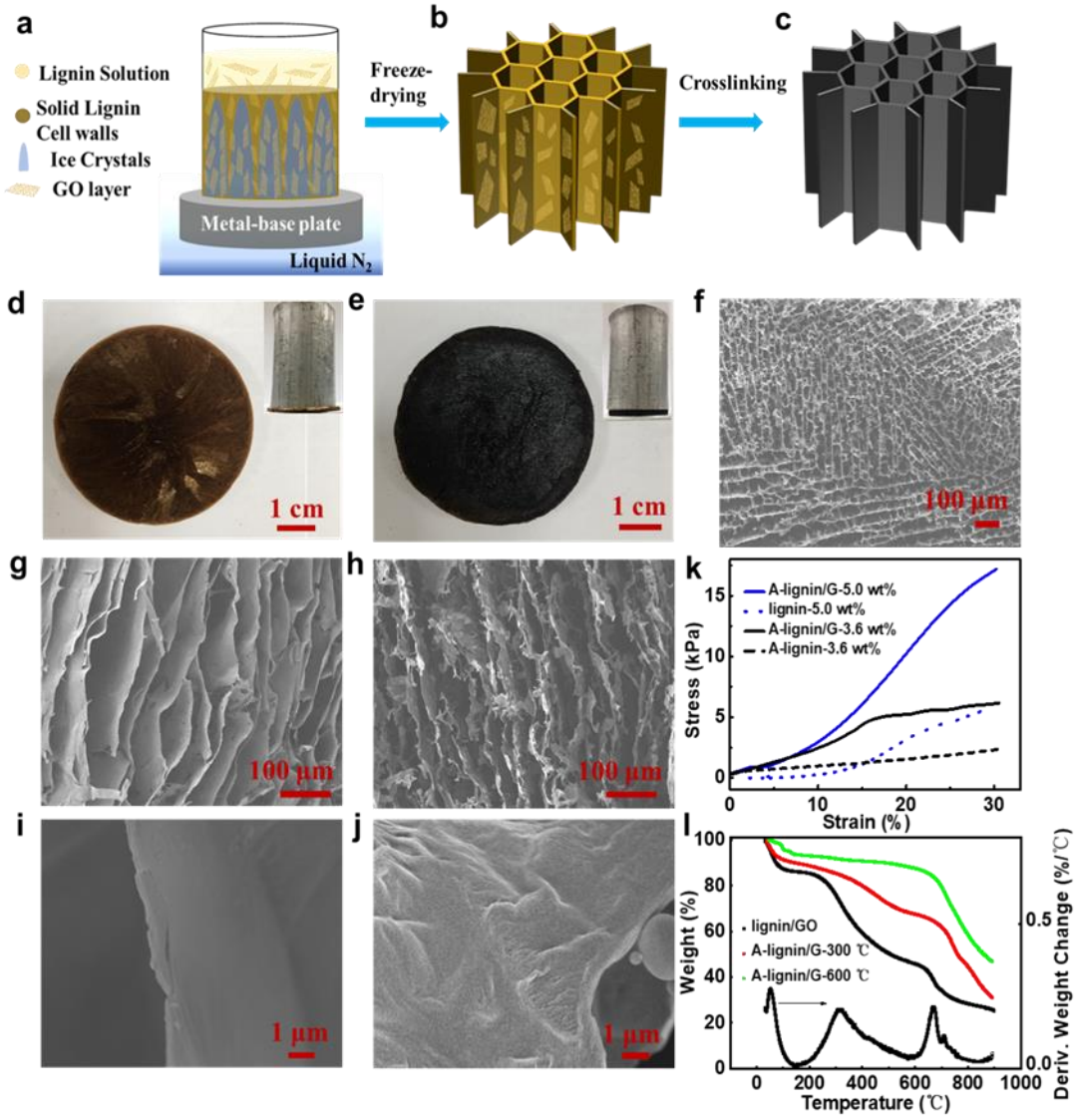

Figure 1. Schemes showing the fabrication process of the wood-like aerogels: (a) unidirectional ice-crystal-induced self-assembly of the lignin/GO suspension, (b) lignin-based aerogels prepared by freeze-drying, (c) cross-linked lignin/graphene (A-lignin/G) aerogels obtained by low-temperature annealing. Photographs of (d) lignin/GO aerogel and (e) A-lignin/G aerogel (the inset show that lignin/GO aerogel is crushed and A-lignin/G aerogels is stable when they are supporting a metal over 2000 times heavier). (f) A SEM image showing porous microstructures of A-lignin/G aerogels with wood-like texture in cross sectional plane. Porous microstructures in longitudinal plane of (g) lignin/GO and (h) A-lignin/G aerogels. Cell walls of (i) lignin/GO and (j) A-lignin/G aerogels. (k) Compressive curves of the aerogels prepared from suspensions of various lignin concentrations. (l) Thermogravimetric analysis traces of the aerogels after annealing at different temperatures.

.

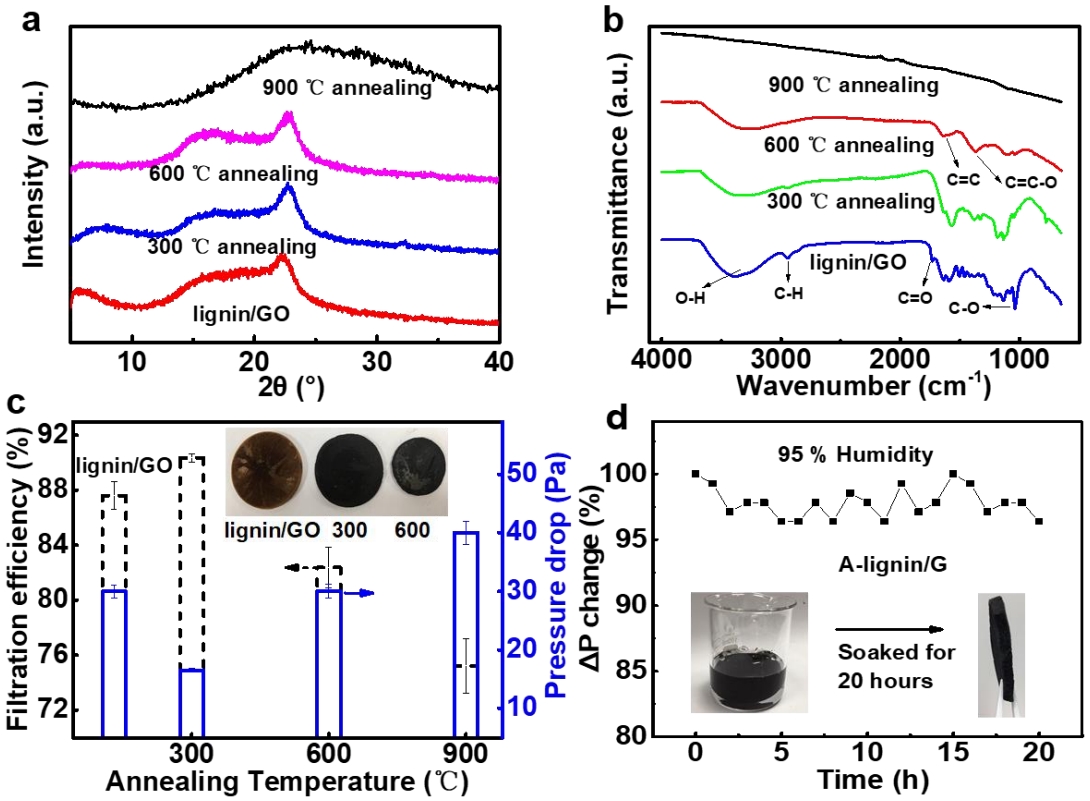

Figure 2. (a) XRD patterns and (b) FTIR spectra of the aerogels before and after cross-linking at various temperatures; (c) filtration efficiency and pressure drop of the 3.6 mm-thick 5.0 w% A-lignin/G aerogels after annealing at various temperatures (the inset shows optical images of the samples annealed at various temperatures); (d) relative pressure drop (ΔP at a certain time/initial ΔP) for the A-lignin/G aerogels annealed at 300 ℃ under humidity of 95 % RH as a function of time (the inset shows the pictures of the aerogels soaked in water and after soaking for 20 hrs, demonstrating the water-resistance of the cross-linked lignin).

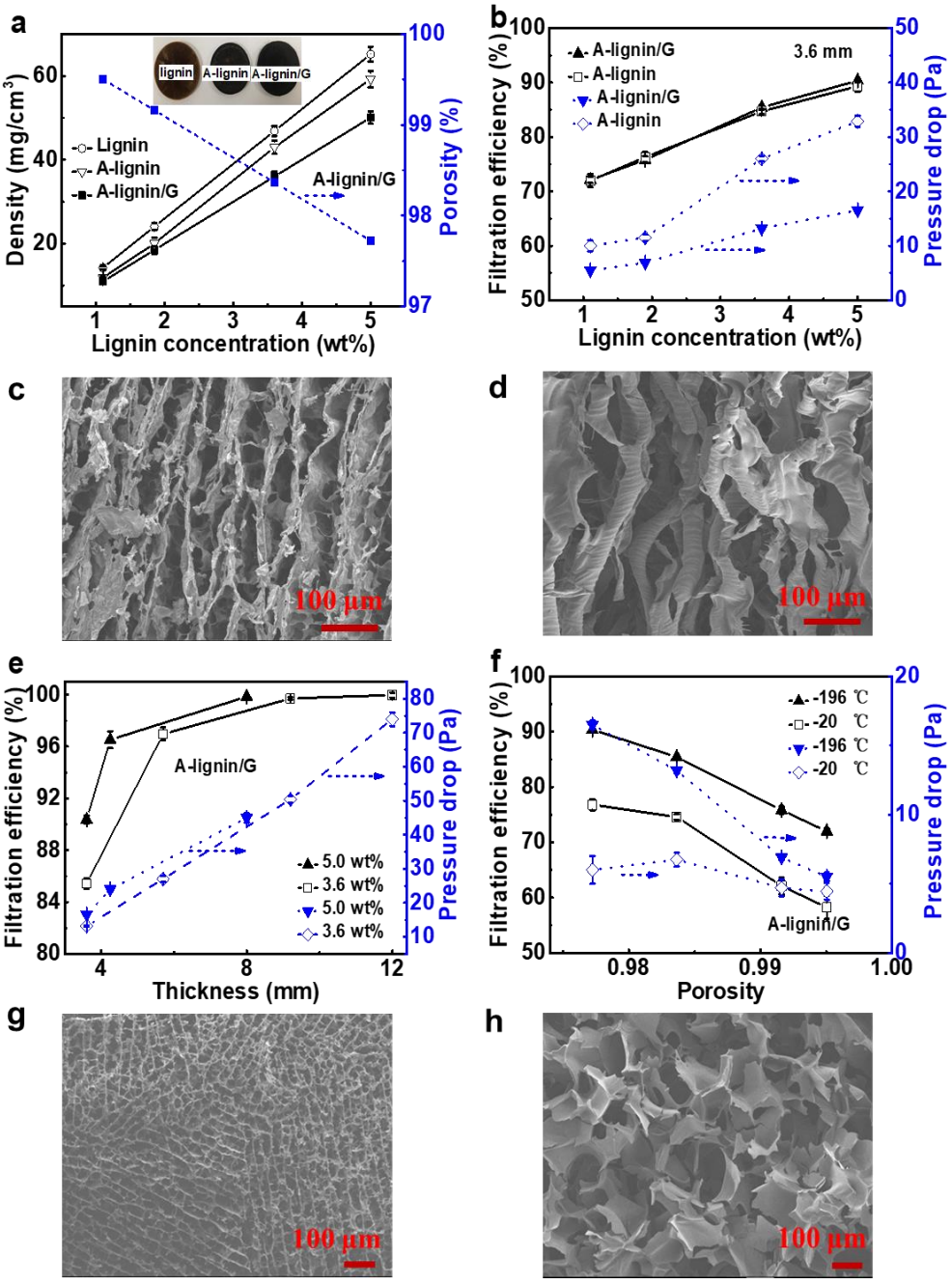

Figure 3. (a) Density and porosity of the lignin-based aerogels prepared from suspensions of various lignin concentrations before and after cross-linking (the inset shows the optical images of the aerogels (from left to right: lignin, A-lignin, and A-lignin/G aerogels). (b) Filtration efficiency and pressure drop of the 3.6 mm-thick A-lignin and A-lignin/G aerogels prepared from suspensions of various lignin concentrations. SEM images showing microstructures of (c) A-lignin/G and (d) A-lignin aerogels. Filtration efficiency and pressure drop of (e) A-lignin/G (prepared from 5 wt% lignin suspension) with various thicknesses, and (f) 3.6 mm-thick A-lignin/G aerogels prepared at different freezing temperatures. Microstructures of A-lignin/G prepared from 5.0 wt% lignin suspension frozen at (g) -20 ℃ and (h) -196 ℃. (A-lignin and A-lignin/G aerogels are annealed at 300 ℃).

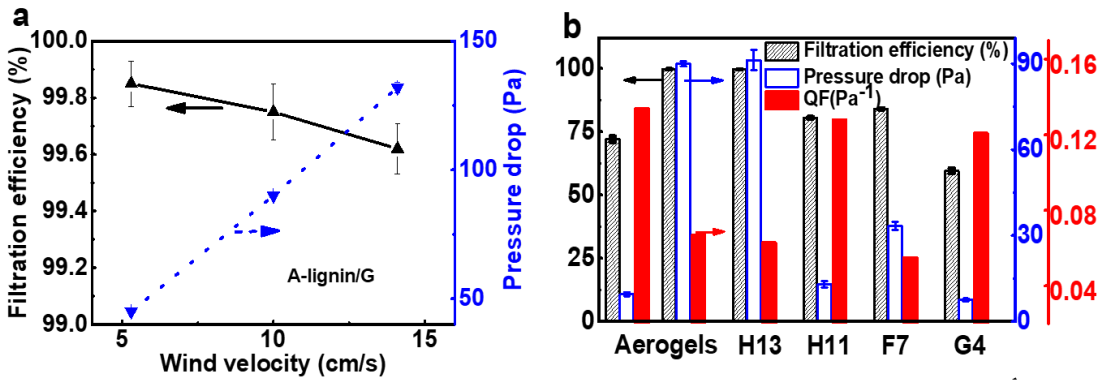

Figure 4. (a) Filtration efficiency and pressure drop of 5.0 wt% A-lignin/G aerogels at a thickness of 8 mm under various wind velocities. (b) Comparison of the filtration efficiency, pressure drop, and QF of A-lignin/G aerogels (the left data is obtained from 1.1 wt% A-lignin/G aerogels at a thickness of 3.6 mm, and the right one is obtained from 5.0 wt% A-lignin/G aerogels at a thickness of 8 mm) and commercial air filters (H13, H11, F7 and G4) at wind velocity of 10.0 cm/s.

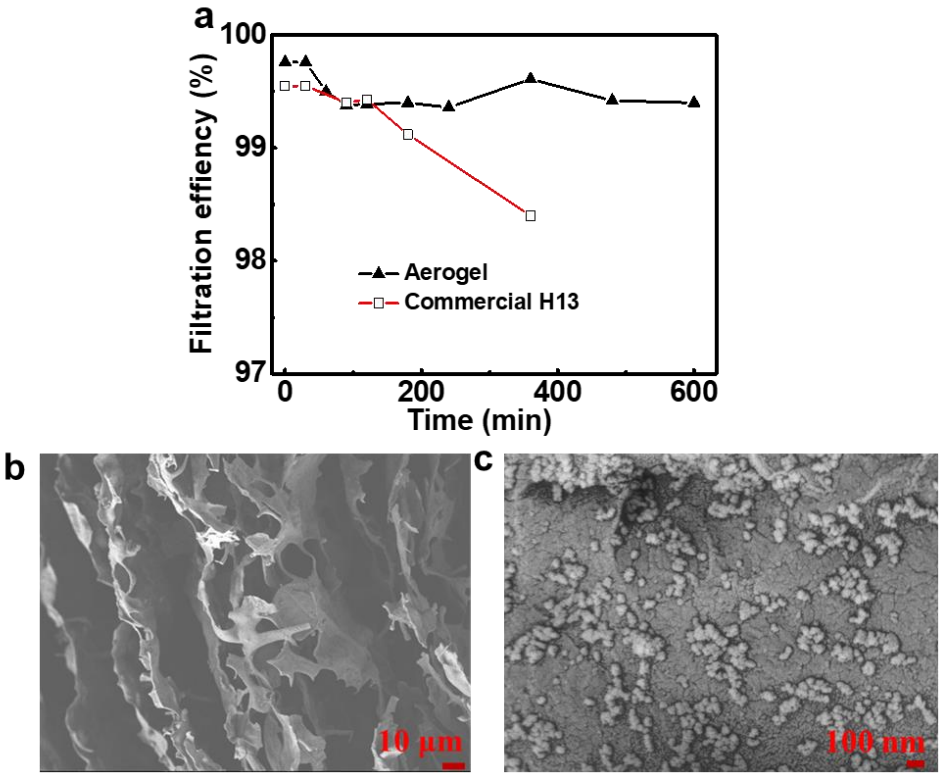

Figure 5. (a) The filtration efficiency of the aerogels and H13 filters as a function of filtration time. The microstructure of the wood-like aerogels after adsorption of model pollutant particles: (b) the well retained pore channels and cell walls and (c) the adsorbed particles.

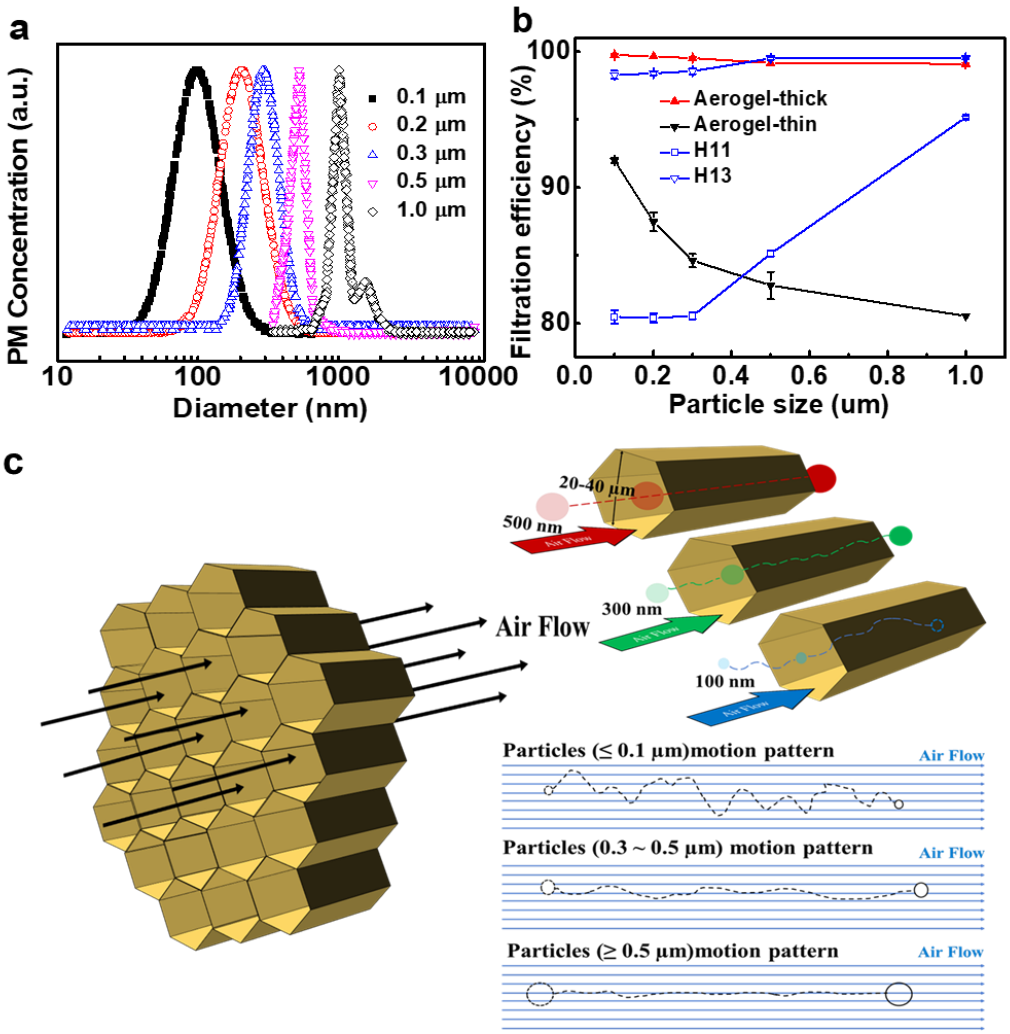

Figure 6. (a) Size distribution curves of model pollutant particles generated from the aerosol generator with peaks at around 0.1, 0.2, 0.3, 0.5 and 1.0 μm, respectively. (b) Filtration efficiency of the wood-like aerogels (the thick and thin aerogels are 5.0 wt% A-lignin/G aerogels at a thickness of 8 and 3.8 mm, respectively) and HEPA filters (H13 and H11) for the particles. (c) Schematics illustrating filtration mechanisms of the wood-like aerogels for particles of different sizes.

For Table of Contents Use Only

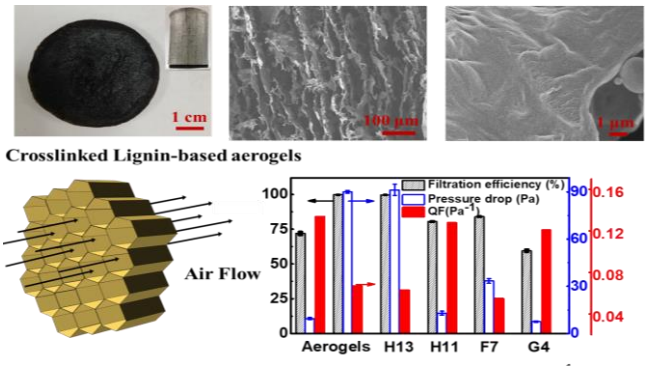

Synopsis

Lignin is utilized to fabricate sustainable aerogel filters for high-efficiency capture of ultrafine airborne particulates, and the mechanism is revealed.